Numerical Modeling for Combustion and Soot Formation Processes in Turbulent Diffusion Flames

Hoo-Joong Kim, Yong-Mo Kim

Department of Mechanical Engineering, Hanyang University, Seoul, 133-791, Korea

In order to investigate the soot formation and oxidation processes, we employed the two variable approach and its source terms representing soot nucleation, coagulation, surface growth and oxidation. For the simulation of the axi-symmetric turbulent reacting flows, the pressure -velocity coupling is handled by the pressure based finite volume method. We also employed laminar flamelet model to calculate the thermo-chemical properties and the proper soot source terms from the information of detailed chemical kinetic model. The numerical and physical models used in this study successfully predict the essential features of the combustion processes and soot formation characteristics in the reacting flow field.

Key Words : Turbulent Diffusion Flame, Laminar Flamelet, Soot Formation and Oxidation

Nomenclature

$M_{C(s)}$: Molecular weight of solid carbon
N_a : Avogadro's number
P : Probability density function
S : Source terms of transport equations
T : Temperature
Z : Mixture fraction
a : Plancks mean absorption coefficient
k : Turbulent kinetic energy
u : Velocity component
x_j : Component in the x and r coordinate direction
Γ : Diffusion coefficient in each transport equation
α, δ : Nucleation rate
β : Coagulation rate
γ : Surface growth rate
χ : Scalar dissipation rate
ε : Dissipation of turbulent kinetic energy
ϕ : Scalar quantity
ρ : Density
σ : Stefan-Boltzmann constant

Subscripts

b : Background value
k : Species index
n : Soot number density
v : Soot volume fraction

* Corresponding Author,
E-mail : ymkim@email.hanyang.ac.kr
TEL : +82-2-2290-0428; **FAX** : +82-2-2297-0339
Associate Professor, Department of Mechanical Engineering, Hanyang University, 17, Haengdang -Dong, Sungdong-Gu, Seoul, 133-791, Korea. (Manuscript **Received** June 11, 2001; **Revised** October 18, 2001)

1. Introduction

In practical combustion devices such as industrial furnaces, gas turbines, or internal combustion engine, most of them use the hydrocarbon fuels and deviate from the ideal conditions under which the combustion of fuel leads to carbon dioxide and water. Therefore, soot is generated as a by-product in the region where the local concentration of oxygen is not sufficient to convert the fuel into water and carbon dioxide. Since this soot emission causes severe environmental damages and human health problems, there is need for better understanding of the processes that are responsible for the formation and oxidation of soot.

While intensive research have been performed over the last decade to understand and model soot formation, there is neither any universal theory nor any model that is applicable to different fuels and a wide range of flow conditions. It is mainly due to complexity of PAH chemical kinetics and

surface reaction. Brookes and Moss(1999) investigated axisymmetric turbulent methane/air jet flames at the atmospheric and an elevated pressure. There are quite detailed measurment data sets in terms of mean mixture fraction, mean temperature, and soot volume fraction. So we selected this experiment as the benchmark case.

In the present study, we used the laminar flamelet approach to model the turbulent combustion processes. The laminar flamelet model views turbulent flame as an ensemble of stationary laminar diffusion flamelets which are stretched and distorted by turbulent flow. This approach gives us the advantage of detailed information on intermediate species and radicals. For the investigated methane/air flame, a library of flamelets has been calculated. The chemical model consists of 32 chemical species and 177 chemical reaction for the methane/air flame. The rate coefficients were taken from GRI-Mech 2.11 and we did not include the NOx production mechanism of the original chemical mechanism. The stationary solutions were stored in a library containing profiles of temperature, density, and mass fractions of all species given as a function of mixture fraction and scalar dissipation rate. We also employed the two variable soot model proposed by Moss et. al(1988) and Lindstedt et. al(1992) because of its simplicity and acetylene treated as a soot precursor. The numerical and physical models used in this study successfully predict the essential features of the combustion processes and soot formation characteristics in reacting flow field.

2. Flow Field Modeling

The density-weighted Navier-Stokes equation, k-ε turbulent model equation, energy equation, and mean and variance of mixture fraction equations are employed to predict the turbulent reacting flow in cylindrical coordinate and represented in general as.

$$\frac{\partial}{\partial t}(\bar{\rho}\bar{\phi})+\frac{\partial}{\partial x_j}(\bar{\rho}\tilde{u}\tilde{\phi})=\frac{\partial}{\partial x_j}\left(\Gamma_\phi\frac{\partial\phi}{\partial x_j}\right)+S_\phi \quad (1)$$

where ϕ may be mean axial and radial velocity, mean enthalpy, turbulent kinetic energy and dissipation rate, mean and variance of mixture fraction Γ_ϕ and S_ϕ represent the diffusion coefficient and source term respectively. In this study, we used the same diffusion coefficients and source terms in Kim et. al, (2000).

The energy conservation equation is solved in terms of enthalpy and its source terms include the effect of thermal radiation. We assume that the flame is optically thin so that radiation source term can be determined locally only by emission. With the assumption of the optically thin limit, the radiative heat loss rate per unit volume can be expressed as

$$Q_{rad}=4\sigma\sum(P_k\cdot a_{P,k})\,(T^4-T_b^4) \quad (2)$$

where σ is the Stefan-Boltzmann constant, P_k is the partial pressure of species k, T is the local flame temperature and T_b is the background temperature. The Planck mean absorption coefficients, $a_{P,k}$ for the k-th radiating gas species are taken from the curve fit value in Computational Submodel Section of International Workshop on Measurement and Computation of Turbulent Nonpremixed Flames(www. ca. sandia. gov/tdf/Workshop/Submodels. html).

The governing equations are solved using a control-volume based finite difference method as an unsteady problem. The present formulation is based on a curvilinear general coordinate with a non-staggered grid. The Second order accurate central differencing scheme is used for the diffusion terms. To reduce numerical diffusion, the second order TVD upwind scheme(Chakravarthy et. al, 1985) for convection terms is implemented. The pressure-velocity coupling is handled by the improved PISO algorithm(Kim et. al, 1994).

3. Laminar Flamelet Approach

The laminar flamelet model views the turbulent flame as an ensemble of stationary laminar diffusion flamelets which are stretched and distorted by turbulent flow. In laminar flamelets, all thermodynamic scalar quantities are a unique function of mixture fraction and scalar dissipation rate. One can obtain the species and energy

equations transformed into flamelet coordinate, namely mixture fraction(Z) and scalar dissipation rate(χ) space, by introducing a Crocco coordinate transformation. Using these transformed equations, we can construct the flamelet library. Here we used the transformed equations with variable Lewis number and scalar dissipation rate in mixture fraction space(Pitsch et. al, 1998).

A library of flamelets has been calculated for the investigated methane/air flame. A flamelet code with an adaptive grid was used to achieve higher precision in the calculations. The chemical model consists of 32 chemical species and 177 chemical reactions for the methane/air flame. The rate coefficients were taken from GRI-Mech 2.11 and we did not include the NOx production mechanism of the original chemical mechanism. The stationary solutions were stored in a library containing profiles of temperature, density, and mass fractions of all species in tems of mixture fraction and scalar dissipation rate.

With the calculated laminar flamelet library, the mean thermo-chemical properties in turbulent reacting flow can be calculated in the following manner,

$$\bar{\phi}=\int_0^\infty \int_0^1 \phi(Z,\chi)P(Z,\chi)\,dZd\chi \qquad (3)$$

where $P(Z,\chi)$ is the joint PDF of mixture fraction and scalar dissipation rate. If the mixture fraction, Z, and scalar dissipation rate, χ, are statistically independent of each other, the joint probability function can be simply written as

$$P(Z,\chi)=P(Z)\cdot P(\chi) \qquad (4)$$

To avoid complications, we used the presumed PDF approach which imply assumption of the shape of the PDF. The most commonly used PDF for the mixture fraction is the beta function distribution and for the scalar dissipation rate, the log-normal distribution(Lentini, 1994).

$$P(Z)=\frac{Z^{a-1}(1-Z)^{b-1}}{\int_0^1 Z^{a-1}(1-Z)^{b-1}dZ} \qquad (5)$$

$$a=\tilde{Z}\left(\frac{\tilde{Z}(1-\tilde{Z})}{\widetilde{Z''^2}}-1\right)\quad b=(1-\tilde{Z})\left(\frac{\tilde{Z}(1-\tilde{Z})}{\widetilde{Z''^2}}-1\right)$$

The mean and variance of mixture fraction are provided by the solution of their transport equations.

$$P(\chi)=\frac{1}{\chi\sigma\sqrt{2\pi}}\exp\left[-\frac{1}{2\sigma^2}(\ln\chi-\mu^2)\right] \qquad (6)$$
$$\tilde{\chi}=\exp(\mu+0.5\sigma^2)\quad \sigma^2=2.0$$

where the mean scalar dissipation rate is modeled as follow :

$$\tilde{\chi}=C_\chi\frac{\tilde{\varepsilon}}{\tilde{k}}\widetilde{Z''^2}\quad C_\chi=2.0 \qquad (7)$$

4. Modeling of Soot Formation

The laminar flamelet model has ability to give us the information of the intermediate species and radicals as a turbulent combustion model. In the flamelet soot modeling, the rate of soot volume fraction instead of the soot volume fraction is expressed as a function of the mixture fraction and the scalar dissipation rate. We used the two -equation model proposed by Moss et. al(1988) and Lindstedt et. al(1992) because of its simplicity. The Favre averaged transport equation of soot number density and soot volume fraction are written as the form of Eq. (1), if we insert the proper scalar variables and its source terms. For soot number density equation(ϕ_n=n/ρNa) and soot volume fraction ($\phi_V=\rho_{soot}f_v/\rho$) of Moss model, the source terms are :

$$\overline{S_{\phi_n}}=\bar{\alpha}-\overline{\beta\rho^2}(\tilde{\phi}_n)^2$$
$$\overline{S_{\phi_v}}=N_a^{1/3}\overline{\gamma\rho}(\tilde{\phi}_n)^{1/3}(\tilde{\phi}_v)^{2/3}+\bar{\delta} \qquad (8)$$

where α and β are nucleation and coagulation rates, respectively. γ is surface growth rate. δ represents the impact of nucleation on the soot mass fraction. The following Arrhenius type expressions have been proposed by Moss et. al (1988) for the rates α, β, γ, and δ.

$$\alpha=C_\alpha\rho^2T^{1/2}X^{m\alpha}\exp(-T_a/T)\quad \beta=C_\beta T^{1/2}$$
$$\gamma=C_\gamma\rho T^{1/2}X^{m\gamma}\exp(-T_\gamma/T)\quad \delta=C_\delta\alpha \qquad (9)$$

T is gas temperature, and X is the soot precursor, C_2H_2 mole fraction. T_a=46.1E3, T_γ=12.6E3, C_α=6.54E4, C_β=1.3E7, C_γ=0.1, and C_δ=144. $m\alpha=m\beta=1$.

For the Lindstedt model, the source terms are:

$$\overline{S_{\phi v}}=\bar{r}_i M_{C(s)}+[\overline{r_{ii}\rho}-\overline{r_{iii}\rho}]M_{C(s)}^{1/3}(\tilde{\phi}_v)^{2/3}(\tilde{\phi}_n)^{1/3}$$
$$\overline{S_{\phi n}}=[\overline{r_{iv}}-\overline{r_v\rho^2}M_{C(s)}^{-1/6}(\tilde{\phi}_v)^{1/6}(\tilde{\phi}_n)^{11/6}]/N_a \quad (10)$$

where the first, second and third source term of soot mass fraction equation represent nucleation, surface growth and O_2 oxidation, respectively. The first and second source term of soot number density equation is the nucleation and coagulation rate. The following Arrhenius type expressions have been proposed by Lindstedt et. al(1992) for each reaction rate.

$$r_i=1.35\times10^6\exp(-20634/T)\,[C_2H_2]$$
$$r_{ii}=5.00\times10^2\exp(-12079/T)f(p)\,[C_2H_2]$$
$$r_{iii}=1.78\times10^2T^{1/2}\exp(-19628/T)f'(p)\,[O_2]$$
$$r_{iv}=\frac{2}{C_{\min}}N_A r_i \quad r_v=2C_a\left(\frac{6M_{C(s)}}{\pi\rho_{C(s)}}\right)^{1/6}\left(\frac{6kT}{\pi\rho_{C(s)}}\right)^{1/2}$$
$$f(p)=\pi\left(\frac{6M_{C(s)}}{\pi\rho_{C(s)}}\right)^{2/3} \qquad f'(p)=\frac{f(p)}{M_{C(s)}}$$

where T is gas temperature, $M_{C(s)}$ is molar mass of soot(12.011kg/kmol), $\rho_{C(s)}$ is soot density (1800kg/m^3), $C_{\min}$ is the number of carbon atoms in the incipient carbon particle(9×10^4), C_a is an coagulation rate constant(3), N_A is Avogadros' number(6.022×10^{26} particles/kmol) and k is Boltzmann constant(1.381×10^{-23} J/K).

We also implemented the OH soot oxidation rate proposed by Bradley et. al(1984). This reaction rate is added in source term of soot mass fraction equation and given as follow :

$$r_{OH}=-0.36T^{1/2}f'(p)\,[OH]\rho M_{C(s)}^{1/3}Y_{C(s)}^{2/3}n^{1/3} \quad (11)$$

5. Results and Discussion

We adopted the experimental measurements of Moss et. al(1999) to validate the present modeling. The experimental conditions are that temperature is 290K for both the fuel and air streams and pressure is 1atm. Fuel is injected through a nozzle of 4. 07mm at a speed of 20. 3m/s. The air stream has a mass flow rate of 707g/min to the chamber. The combustion chamber diameter is 155mm. Calculation of the governing equation is performed in the cylindrical coordinate system. The governing equations in this computational domain were discretized by the grid system with 98 and 100 points in axial and radial direction, respectively.

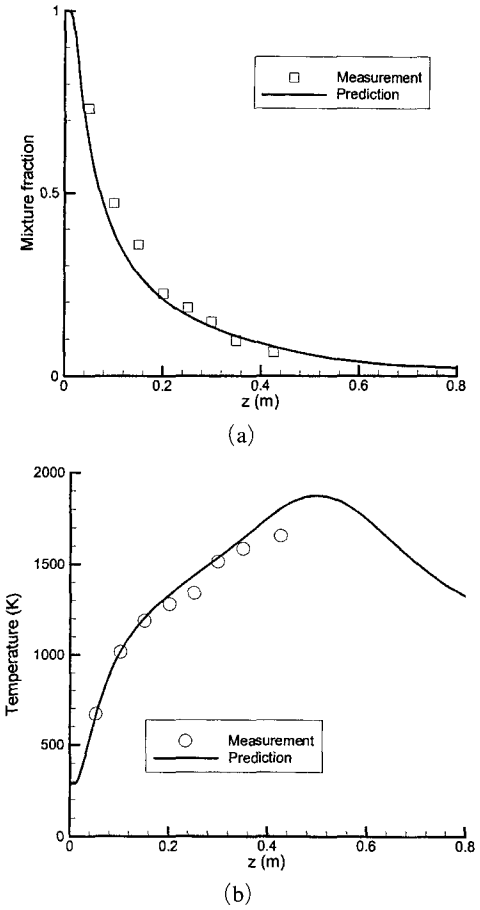

Fig. 1 Axial profiles of (a) mean mixture fraction and (b) mean temperature

Figure 1 shows the centerline profiles of mean mixture fraction and mean temperature. Mean mixture fraction decreases while mean temperature increases along the centerline. Near the flame tip region, overprediction of temperature is observed although agreements are generally good.

We investigated the scalar field, mean mixture fraction and temperature field, in order to validate the models in the present study. Figure 2 represents the radial profiles of mean mixture fraction at some axial locations (i. e. z=150, 200, 250, 300, 350, 425mm). The experimental values are well reproduced except the centerline downstream region (z>300mm). The radial profiles of mean temperature are shown in Fig. 3 at some axial locations. Calculation of thermo-chemical

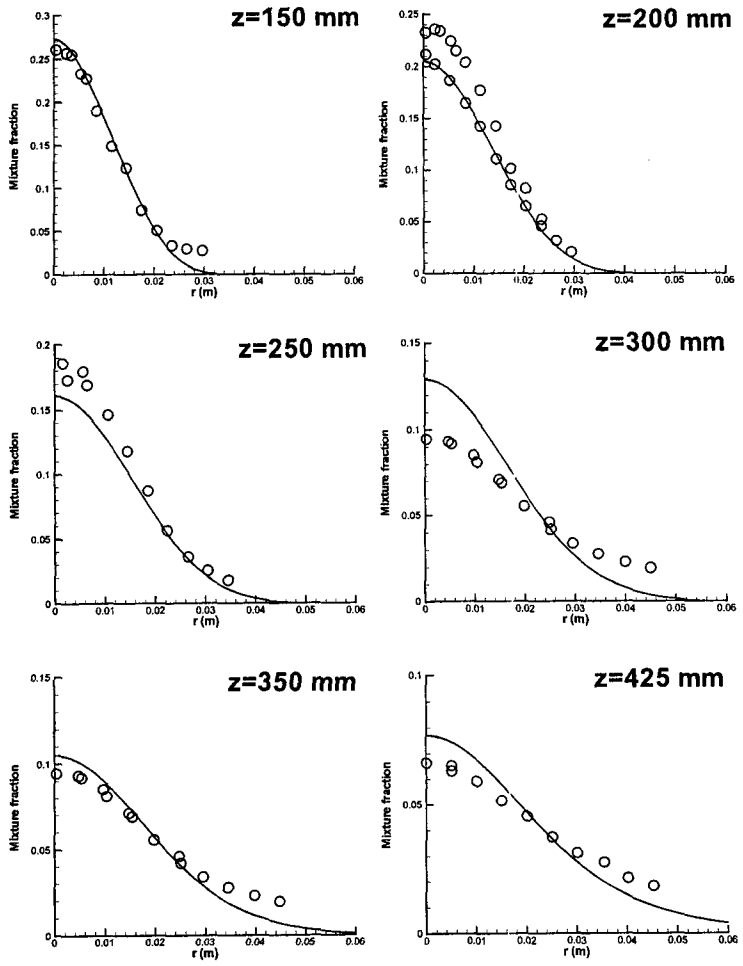

Fig. 2 Radial profiles of mean mixture fraction at some axial positions. (Symbols ; measurements, Lines ; predictions)

scalar quantities is carried out using the flamelet library and presumed PDF. In the region of z> 350mm, over predicted temperature occurs near the centerline. However, the predicted temperatures agree with the measured values with good prediction of the radial location of the peak temperature at each axial location. So, we conclude that the laminar flamelet model has good prediction ability for calculating the scalar fields such as mean mixture fraction, mean temperature etc..

Figure 4 shows the fields of mean temperature and acetylene which has been treated as soot precursor. Temperature has its maximum value in the flame tip region and peak temperature exist along the stoichiometric line. Acetylene has its maximum concentration in the upstream region (z≅280mm) of maximum temperature region. The overall distribution of acetylene shows that higher acetylene concentration is in the fuel rich region.

The soot number density, mass fraction and its source terms are shown in Fig. 5. Since soot nucleation rate is not only dependent on acetylene concentration but also temperature, it has its maximum value not in the region of maximum acetylene concentration but in the region (z≅ 260mm, r≅15mm) where high temperature and acetylene concentration coexist. Soot surface growth rate has maximum value in the slightly

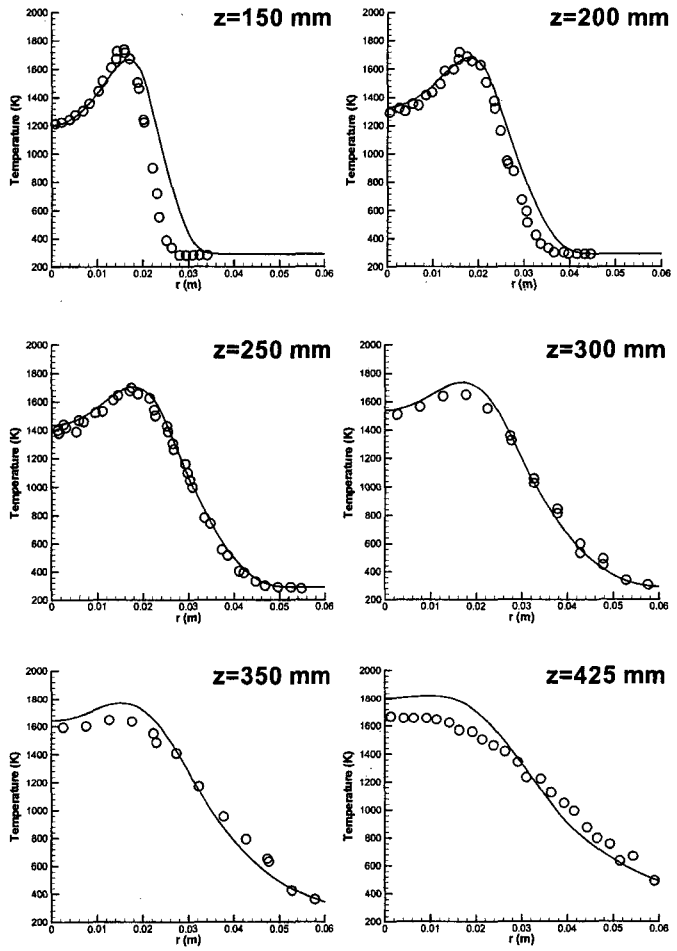

Fig. 3 Radial profiles of mean temperature at some axial positions. (Symbols ; measurements, Lines ; predictions)

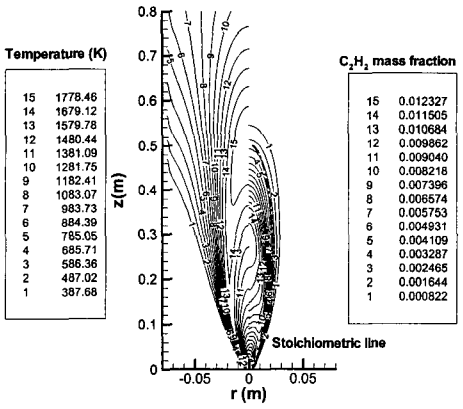

Fig. 4 Mean temperature and acetylene mass fraction fields. Dashdot line denotes the stoichiometric line

downstream of maximum nucleation rate region. Because it is not only dependent on the acetylene concentration but also proportional to the soot surface area, high number density leads to the high surface growth rate. O_2 and OH oxidation rate is also proportional to the soot surface area so that they have maximum rates in the high soot number density region. OH oxidation rate has peak values along the high temperature region due to its high concentration in that region. The generated soot particles are transported to the downstream region and its size is increased by soot surface growth and decreased by surface oxidation. Near z=370mm, soot mass fraction has maximum value. As soot particle moves to-

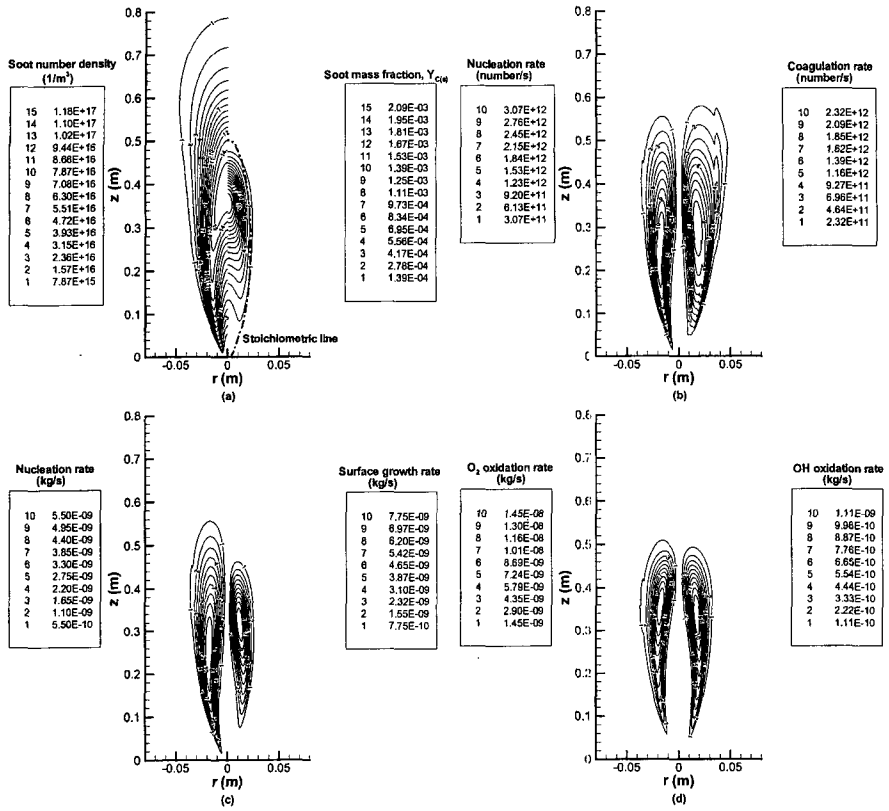

Fig. 5 The distribution of soot number density, soot mass fraction and its source terms

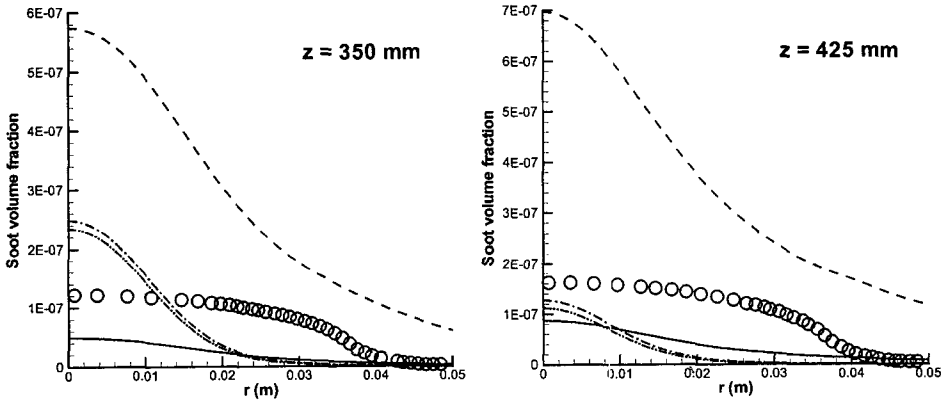

Fig. 6 Radial profiles of soot volume fraction at some axial location. Symbol dentoes the meausred value. Lines denote prediction ; solid (Moss model), dashed (Lindstedt model included nucleation and surface growth), dashdot (Lindstedt model included nucleation, surface growth and O_2 oxidation), dashdotdot (Lindstedt model included nucleation, surface growth, O_2 oxidation and OH oxidation)

ward downstream and radial region of its maximum mass fraction place, soot particle is oxidized and soot mass fraction is decreased rapidly. Most of soot particles exist in the fuel rich condition. Since coagulation rate is not only proportional to temperature and number density but also proportional to the square root of soot diameter, it has maximum value in slightly down-

stream of maximum nucleation rate location. We understand that maximum coagulation location does not coincide with maximum soot number density region and this mainly results from the decrease of soot diameter by surface oxidation.

Figure 6 shows the radial profiles of soot volume fraction at z=350 and 425mm. The results of Moss model have larger underprediction than Lindstedt model. To achieve the better prediction, modifications of model constant in Moss model are needed. Only considering soot nucleation and surface growth of Lindstedt model, we have large over-prediction in entire radial range. The predicted value is approaching to the measured value due to including soot surface oxidation. The soot oxidation rate is higher in downstream than upstream region. Because OH soot oxidation rate is much less than O_2 oxidation rate, the effect of OH soot oxidation on the soot volume fraction is small. But OH oxidation results in the decrease of soot volume fraction near the centerline. The prediction of soot volume fraction has good level for comparison with the measured value. But overprediction is in the upstream and underprediction is in the downstream. The width of soot distribution is underpredeicted because the oxidation rate is higher than the surface growth rate.

6. Conclusions

Numerical modeling of turbulent combustion and soot formation is presented in this paper. We used the density weighted Navier-Stokes equations and standard k-ε turbulent model equations to model turbulent flow field and mixture fraction equation, laminar flamelet model and presumed PDF(beta function for mixture fraction and log-normal function for scalar dissipation rate) approach to solve the mean reaction rate. We also used the two equation model representing soot number density and soot mass fraction and its source terms which include the acetylene concentration as a soot precursor.

The models used show good agreement with the experimental distributions and good capability to predict scalar quantities such as temperature and mean mixture fraction. Nucleation rate has the maximum value in the region where high temperature and acetylene concentration coexist due to its dependency on temperature and acetylene concentration. Generated soot particles are transported downstream and oxidized by oxygen and OH species. As soot particles go through the oxidation zone, the soot mass fraction and particle diameter decrease rapidly. The peak coagulation location does not coincide with the peak soot number density region due to decrease of soot diameter by surface oxidation. Most of soot exist in the fuel rich region. The soot oxidation rate is higher in the downstream than upstream region. The effect of OH soot oxidation on the soot volume fraction is small because the OH soot oxidation rate is much less than O_2 oxidation rate. But OH oxidation results in decrease of the soot volume fraction near the centerline. Predicted soot volume fraction shows good comparison with the measured values, in spite of overprediction in the upstream region and underprediction in the downstream region. The width of soot distribution is underpredeited because of the oxidation rate higher than the surface growth rate.

References

Bradley, D., Dixon-Lewis, G., El-Din Habik and Mushi, E. M. J., 1984, *20th Symposium (International) on Combustion, The Combustion Institute*, p. 931.

Brookes, S. and Moss, J. B., 1999, "Measurement of Soot Production and Thermal Radiation from Confined Turbulent Jet Diffusion Flames of Methane," *Combust. and Flame*, Vol. 116, pp. 49~61.

Chakravarthy, S. R., and Osher, S., 1985, AIAA-85-0363, 23rd Aerospace Sciences Meeting, Reno, NV.

Fairweather, M., Jones, W. P., and Lindstedt, R. P., 1992, "Predictions of Radiative Transfer from a Turbulent Reacting Jet in a Cross-Wind," *Combust. and Flame*, Vol. 89, pp. 45~63.

http://www. ca. sandia. gov/tdf/Workshop/Submodels. html

Kim, S. K. and Kim, Y. M., 2000, "Prediction of Detailed Structure and NOx Formation Characteristics in Turbulent Nonpremixed Hydrogen Jet," *Combust. Sci. and Tech, Vol.* 156, pp. 107~137.

Kim, Y. M., Chen, C. P., Ziebarth, J. P., and Chen, Y. S., 1994, *Numerical Heat Transfer*, vol. 25, pp. 21~42.

Lentini, D., 1994, "Assessment of the Stretched Laminar Flamelet Approach for Nonpremixed Turbulent Combustion," *Combust. Sci. and Tech.*, Vol. 100, pp. 95~122.

Moss, J. B., Stewart, C., Syed, K., 1988, "Flowfield modeling of Soot formation at elevated pressure," 22nd Symposium (International) on Combustion, The Combustion Institute, pp. 413~423.

Pitsch, H. and Peters, N., 1998, "A Consistent Flamelet Formulation for Non-Premixed Combustion Considering Differential Diffusion Effects," *Combust. and Flame*, Vol. 114, pp. 26~40.